

Estimating Actual Evapotranspiration using the SEBAL Model for the Atankwidi and Afram Catchments in Ghana

Tayari Salifu*†, Wilson Agyei Agyare‡, Nicholas Kyei-Baffour‡,
Ebenezer Mensah‡ and Emmanuel Ofori‡

†*Department of Agricultural Engineering,
Bolgatanga Polytechnic, Bolgatanga, Ghana*

‡*Department of Agricultural Engineering,
Kwame Nkrumah University of Science and Technology (KNUST),
Kumasi, Ghana*

Abstract

Evapotranspiration (ET) monitoring has important implications on global and regional climate modelling. It is important for the hydrological cycle and assessment of environmental stress that affects ecosystems. Accurate measurement and estimation of ET is a basic input in computing water balance and to estimate water availability and requirements. Most methods for ET computation can only provide point estimates of ET for a specific location and fails to provide ET on a regional scale and makes it inadequate for proper water resource management. In this study, the Surface Energy Balance Algorithm for Land (SEBAL) model is used to estimate actual evapotranspiration (ET_a) for different land use/cover types (closed woodlands, gallery forests, open woodlands, farmlands, water bodies, barelands, rocky areas and built-up areas) for the Atankwidi and Afram catchments in the Volta Basin of Ghana. It was found that the SEBAL model can successfully estimate and distinguish ET_a among different land use/cover types in the two catchments. SEBAL estimates of ET_a varied from 1.4 to 7.30 mm/day across the different land use/cover types. The range of CVs for ET_a was 5–75% across the different land use/cover types for the two catchments. The results confirms SEBAL is an appropriate algorithm for estimating ET_a using satellite images in catchments similar to that of the study areas, where few or no ground measurements are available.

Keywords: Evapotranspiration; Landsat; Land use; Remote sensing; SEBAL; Model.

Introduction

Background

Sustainable food production and industrial development depend to a large extent on the judicious use of water resources, as fresh water for human consumption and agriculture is becoming increasingly scarce. Countries with limited water and land resources are faced with greater challenges. The dependency on water for future development has become a critical constraint especially in arid and semi-arid regions, where it is estimated to have water scarcity by the year 2025 [1]. The situation is aggravated by continuous human activities. There is an urgent need to arrest this human-induced degradation of soil and water resources and reclaim those that have already been degraded in order to meet the present and future needs of mankind. There is the need for sustainable use of water resources with respect to different land use patterns. A good understanding and description of the dynamics of a local/regional/global hydrologic cycle as affected by natural and human activities is the starting point for effective management of water resources of a given basin or region [2].

Evapotranspiration (ET_a) is an important component of the water cycle. It is the term used to describe the transfer of water from a variety of surfaces into the atmosphere [3]. It is a process that results from complex interaction between water and energy fluxes subjected to changing atmospheric, soil and vegetation conditions. ET_a constitutes an important component of the water fluxes of the hydrosphere and the atmosphere. An estimated 70% of the water loss from the earth's surface occurs through evaporation. On the global scale, ET_a represents more than 60% of precipitation inputs [Vorosmarty et al].

The complexity associated with the estimation of ET_a has led to the development of various methods for estimating this parameter over time [5]; [Allen et al]. These methods for estimating ET_a can generally be grouped into four (4) categories. These include hydrological methods (water balance), direct measurement (lysimeters), micrometeorological (energy balance) and empirical or combination methods based on energy balance or climatic factors [7]. Most of these methods can only provide point estimates of ET_a which are not sufficient for basin-level water resource management. Also, most of these ET_a computation and measurement methods are limited since they only provide point values of ET_a for a specific location and they fail to provide ET_a on a regional scale. Data collection for ET_a computations is sometimes difficult or even impossible due to inaccessibility of the area in question. During the last two to three decades, significant progress has been made to estimate ET_a using satellite remote sensing [8]; [9]; [Bastiaanssen et al]; and [Kustas et al].

The SEBAL is a remote sensing algorithm used to compute the surface energy balance on an instantaneous time scale and for each pixel of a satellite image [Bastiaanssen et al]. It has been used for many studies including water balance estimations [12]; irrigation performance assessment studies [13], and for weather prediction studies [Van de Hurk et al]. The model has been applied in different basins of the world, e.g., Snake River basin in Idaho, USA [Allen et al], the Lake Naivasha drainage basin in Kenya [16], All river basins in Sri Lanka [17] and the Indus Basin in Pakistan [Bastiaanssen et al].

In Ghana, [19] successfully used the SEBAL model to compute ET_a in the Volta Basin, Navrongo, Upper East Ghana. In addition, [Compaore' et al] used the SEBAL model to map evaporation in the White Volta Basin of Ghana, West Africa using Landsat and MODIS images.

In this study the SEBAL model is used to estimate ET_a for different land use/cover types in the Atankwidi and Afram catchments in Ghana. Using this method, energy balance is applied at each pixel to map spatial variation of ET_a .

The Surface Energy Balance Algorithm for Land (SEBAL) model

The SEBAL method is based on the computation of surface albedo, surface temperature and NDVI [21] from multispectral satellite data. The surface albedo is calculated from Thematic Mapper bands 1-5 and 7; the surface temperature from band 6; the vegetation index from bands 3 and 4. The surface albedo is used to calculate net short wave radiation, and surface temperature for the calculation of net long wave radiation, soil heat flux and sensible heat flux. The vegetation index governs the soil heat flux by incorporating light interception effects by canopies and is used to express the aerodynamic roughness of the landscape [19].

The SEBAL is a physically based analytical method that evaluates the components of the energy balance and determines the ET_a rate as the residual [22]. By the law of conservation of energy, the equation for the inputs, losses, and storage of energy for a surface on earth is expressed by Eq. (1) [23]:

$$R_n = G + H + \lambda ET \text{ (W/m}^2\text{)} \tag{1}$$

Where R_n is the net radiation flux at the surface, G is the soil heat flux, H is the sensible heat flux to the air, and λET is the latent heat flux.

The net radiation is estimated based on Eq. (2) [10]:

$$R_n = R_{S\downarrow} (1-\alpha) + R_{L\downarrow} - R_{L\uparrow} - R_{L\downarrow}(1- \epsilon_o) \text{ (W/m}^2\text{)} \tag{2}$$

where $R_{S\downarrow}$ (W/m²) is the incoming direct and diffuse shortwave solar radiation that reaches the surface; α is the surface albedo, the dimensionless ratio of reflected radiation to the incident shortwave radiation; $R_{L\downarrow}$ is the incoming long wave thermal radiation flux from the atmosphere (W/m²); $R_{L\uparrow}$ is the outgoing long wave thermal radiation flux emitted from the surface to the atmosphere (W/m²); ϵ_o is the surface emissivity, the (dimensionless) ratio of the radiant emittance from a greybody to the emittance of a blackbody.

The surface albedo is computed using Eq. (3).

$$\alpha = \frac{\alpha_{toa} - \alpha_{path_radiance}}{\tau_{sw}^2} \tag{3}$$

where; $\alpha_{path_radiance}$ is the average portion of the incoming solar radiation across all bands that is back-scattered to the satellite before it reaches the earth's surface, and

τ_{sw} is the atmospheric transmissivity. Values for $\alpha_{path_radiance}$ range between 0.025 and 0.04 and for SEBAL a value of 0.03 is recommended by [24].

Atmospheric transmissivity is defined as the fraction of incident radiation that is transmitted by the atmosphere and it represents the effects of absorption and reflection occurring within the atmosphere. τ_{sw} includes transmissivity of both direct solar beam radiation and scattered radiation to the surface and is calculated assuming clear sky and relatively dry conditions using an elevation-based relationship from Eq. (4) [6]:

$$\tau_{sw} = 0.75 + 2 \cdot 10^{-5} \cdot z \quad (4)$$

Where; z is the elevation above sea level in meters.

The albedo at the top of the atmosphere (α_{toa}) is computed by Eq. (5):

$$\alpha_{toa} = \sum (\omega_{\lambda} \times \rho_{\lambda}) \quad (5)$$

where; ρ_{λ} is the reflectivity and ω_{λ} is a weighting coefficient for each band

The weighting coefficient for each band is computed by Eq. (6).

$$w_{\lambda} = \frac{ESUN_{\lambda}}{\sum ESUN_{\lambda}} \quad (6)$$

ω_{λ} is the weighting coefficient and $ESUN_{\lambda}$ is the mean solar exo-atmospheric irradiance for each band in $W/m^2/\mu m$

The reflectivity for each band (ρ_{λ}) is computed using Eq. (7) for Landsat images:

$$\rho_{\lambda} = \frac{\pi \cdot L_{\lambda}}{ESUN_{\lambda} \cdot \cos \theta \cdot d_r} \quad (7)$$

where; L_{λ} is the spectral radiance for each band, $\cos \theta$ is the cosine of the solar incidence angle (from nadir), and d_r is the inverse squared relative earth-sun distance d_r is computed using Eq. (8) [6]:

$$d_r = 1 + 0.033 \cos \left(DOY \frac{2\pi}{365} \right) \quad [8]$$

where; DOY is the sequential day of the year and the angle ($DOY \times 2\pi/365$) is in radians.

The spectral radiance for each band (L_{λ}) is the outgoing radiation energy of the band observed at the top of the atmosphere by the satellite. It is calculated using Eq. (9) for Landsat 5 and 7:

$$L_{\lambda} = \left(\frac{L_{MAX} - L_{MIN}}{QCALMAX - QCALMIN} \right) \cdot (DN - QCALMIN) + L_{MIN} \quad (9)$$

where; L_λ is the spectral radiance for each band in $W/m^2/sr/\mu m$, DN is the digital number of each pixel, LMIN and LMAX are calibration constants, QCALMIN and QCALMAX are the highest and lowest range of values for rescaled radiance in DN.

For Landsat 5, QCALMAX = 255 and QCALMIN = 0 so Eq. (9) becomes;

$$L_\lambda = \left(\frac{L_{MAX} - L_{MIN}}{255} \right) \cdot DN + L_{MIN} \quad (10)$$

Landsat 7 ETM+ images provide calibration constants in the header files of each satellite image. The spectral radiance (L_λ) for each band is calculated by Eq. (11) [25]:

$$L_\lambda = gain \cdot DN + offset \quad (11)$$

The NDVI is the ratio of the differences in reflectivities for the near-infrared band (ρ_4) and the red band (ρ_3) to their sum. It is computed using Eq. (12).

$$NDVI = (\rho_4 - \rho_3) / (\rho_4 + \rho_3) \quad (12)$$

The surface temperature (T_s) is calculated using the modified Plank equation Eq. (13)

$$T_s = \frac{K_2}{\ln \left(\frac{\epsilon_{NNB} K_1}{R_c} + 1 \right)} \quad (13)$$

Where T_s is the effective at-satellite temperature in Kelvin, K_1 and K_2 are calibration constants for Landsat images, R_c is the corrected thermal radiance from the surface and ϵ_{NNB} is the narrow band emissivity (0.98 for NDVI > 0 or 0.99 for NDVI < 0). Units for R_c are the same as that for K_1 .

The corrected thermal radiance from the surface (R_c) is calculated using Eq. (14) [Wulkelic et al] as:

$$R_c = \frac{L_{t,b} - R_p}{\tau_{NB}} - (1 - \epsilon_{NB}) R_{sky} \quad (14)$$

where; ϵ_{NB} is the narrow band emissivity, R_c is the corrected thermal radiance from the surface in $W/m^2/sr/\mu m$, $L_{t,b}$ is the spectral radiance in $W/m^2/sr/\mu m$, R_p is the path radiance in the 10.4–12.5 μm band in $W/m^2/sr/\mu m$, R_{sky} is the narrow band downward thermal radiation for a clear sky in $W/m^2/sr/\mu m$, and τ_{NB} is the narrow band transmissivity of air (10.4–12.5 μm).

The soil heat flux (G) is the rate of heat storage to the ground from conduction. Studying irrigated agricultural regions in Turkey, [24] suggested an empirical relationship for G given as:

$$G = R_n T_s / \alpha (.0038 \alpha + .0074 \alpha^2) (1 - .98NDVI^4) (W/m^2) \quad (15)$$

Where T_s is the surface temperature ($^{\circ}\text{C}$), α is the surface albedo (dimensionless), and NDVI is the normalized difference vegetation index (dimensionless).

The most difficult and critical factor in physically based remote sensing algorithms is to solve the equation for the sensible heat flux (H) [Brutsaert et al] and the most difficult issue in the SEBAL model is how to estimate the parameters needed for estimation of the sensible heat flux. The SEBAL sensible heat flux calculations are based on the Monin-Obukov similarity theory that takes into account the effects of atmospheric stability and aerodynamic resistance for heat transport (r_{ah}) [28]. Using the equation for heat transport, sensible heat flux can be calculated by Eq. (16) [23]:

$$H = (\rho c_p dT) / r_{ah} \quad (16)$$

Where ρ is the density of air (kg/m^3), c_p is the specific heat of air (1004 J/kg/K), dT is the difference in temperature between the surface and the air (K), and r_{ah} is the aerodynamic resistance (s/m) which is affected by wind speed, atmospheric stability, and surface roughness [29]. The sensible heat flux is calculated using an iterative process and detailed information on the computation are found in Hong [28].

With R_n , G , and H known, the latent heat flux is the remaining component of the surface energy balance to be calculated by SEBAL. Rearranging Eq. (1) gives the latent heat flux where:

$$\lambda ET = R_n - G - H \text{ (W/m}^2\text{)} \quad (17)$$

Dividing the above equation by the latent heat of vaporization (λ) allows a solution for ET.

The instantaneous latent heat flux, λET , is the calculated residual term of the energy budget, and it is then used to compute the instantaneous evaporative fraction, EF (Eq. (18)):

$$EF = \frac{\lambda E}{\lambda E + H} = \frac{\lambda E}{R_n - G_0} \quad (18)$$

EF expresses the ratio of the actual to the crop evaporative demand when the atmospheric moisture conditions are in equilibrium with the soil moisture conditions. The instantaneous value can be used to calculate the daily value because evaporative fraction tends to be constant during day time hours, although the H and λE fluxes vary considerably. The difference between the instantaneous evaporative fraction at satellite overpass and the evaporative fraction derived from the 24-hour integrated energy balance is marginal and may be neglected according to [30], [31], [16] and [Farah et al]. For time scales of 1 day or longer, G_0 can be ignored and net available energy ($R_n - G_0$) reduces to net radiation (R_n).

The SEBAL model yields an estimate of LE [Wm^{-2}] at the time of the satellite overpass. However, for most hydrological applications the daily total LE (daily ET) is needed; so the instantaneous LE needs to be extrapolated to the daily LE. The extrapolation is done using the evaporative fraction (EF) which has been shown to be

approximately constant during the day Eq. (19) [Shuttleworth et al], [30], [31].

$$EF_{inst} = \frac{R_n - G - H}{R_n - G} = \frac{LE_{inst}}{LE_{inst} + H_{inst}} \approx EF_{24} \quad (19)$$

Therefore, multiplication of the instantaneous EF (EF_{inst}) determined from SEBAL with the total daily available energy yields the daily ET rate in mm/day (Eqs. (20) and (21)) [Bastiaanssen et al].

$$LE_{24} = EF_{inst} \cdot (R_{n24} - G_{24}) \quad (20)$$

and

$$ET_{24} = \frac{EF_{inst} \cdot (R_{n24} - G_{24})}{\lambda} \quad (21)$$

The study area

The study was carried out in the Atankwidi and Afram catchments in the Volta Basin of Ghana. The Atankwidi flows south from Burkina Faso into the Upper East Region of Ghana between Navrongo and Bolgatanga. The Ghanaian part of the catchment covers an area of 159 km². The predominant occupation is rain-fed subsistence farming with shallow ground water along stream and river channels during the dry season [34]. The Afram River is a tributary to the Main Volta, starting from the Ejura-Sekyedumase District in the Ashanti Region of Ghana and flowing eastwards into the Volta. The area of the Afram catchment is about 300 km² with agriculture being the principal occupation of the inhabitants.

The long-term mean annual rainfall in the Atankwidi catchment is 990 mm. The average temperature is 29°C. Relative humidity is highest (65%) during the rainy season and drops quickly at the end of the rainy season to a value of less than 10% during the Harmattan period in December and January [34]. It is in the Sudan savannah, characterised by few and scattered trees such as the baobab, locust bean, acacias and sheanut [37]. Soils in the catchment consist of Lithic leptosols, fluvisols, Gleyic lxisols and Haplic arenosols [38].

The Afram catchment is characterized by two rainy seasons [35] and the mean annual rainfall is about 1300 mm with a very high annual and monthly variability [36]. The average temperature is 26.6 °C, with the highest mean monthly temperature in March just before the onset of the rains. Relative humidity in the Afram catchment is usually more than 90% during the night and early morning. It is of the transitional forest-savannah ecology, which lies between the Guinea savannah zone to the north and the forest vegetation to the south. The vegetation is composed of short branching trees, predominantly less than 15 meters high, which do not usually form a closed canopy and are widely scattered [37]. The soils consist of Dystric leptosols, Ferric lxisols, Haplic luvisols and Dystric fluvisols [36].

Materials and methods

Field data collection and parameter extraction

For the purpose of this study, three (3) landsat images for each catchment were used (Table 1). These were downloaded from the University of Maryland and United States Geological Survey (USGS) websites.

Table 1: Dates of Landsat images used for the study.

Date of image	Catchment	Path/Row
11/11/1989	Atankwidi	194/53
7/11/1999	Atankwidi	194/53
7/11/2005	Atankwidi	194/53
11/1/1986	Afram	194/54
20/03/2002	Afram	194/54
13/01/2007	Afram	194/53

Field identification of land use/cover types

In order to identify the different land use/cover types in the two catchments, field work was undertaken from November 1, 2009 to November 13, 2009 at the Atankwidi catchment and from March 15, 2010 to March 31, 2010 at the Afram catchment. Different land use/cover types were mapped using a hand-held Global Positioning System (GPS) unit. Careful selection was done so as to obtain even distribution of mapping points for each land use/cover over the catchment. Five (5) GPS points corresponding to each selected land use/cover type were taken.

Extraction of actual evapotranspiration maps

To generate the actual evapotranspiration maps for the two catchments, the SEBAL Level 1 Flat Model developed by the Hendrickx's research group at New Mexico Tech was implemented [Compaore' et al]. It consists of several Erdas Imagine models and Microsoft Excel spreadsheets. This was achieved through a series of steps using the Erdas Model Maker tool to compute the terms of the energy budget.

In order to compute the surface albedo (Eq. (3)), the spectral radiance (Eq. (9)) is first computed for each short wave band based on the digital number of each individual pixel. This is followed by the computation of the at-satellite reflectance (Eq. (7)) for each band. The albedo at top of atmosphere (Eq. (5)) is then computed which is also used as an input file to compute the surface albedo (Eq. (3)). The at-satellite reflectance (Eq. (7)) is used to compute the NDVI based on Eq. (12). The spectral radiance computed from Eq. (9) is first used to compute the surface broad band surface emissivity. This is then used to compute the brightness temperature which is also used as an input file in calculating the surface temperature (Eq. (13)).

In order to compute the ET_a , an iteration process described by [28] is first used to compute the sensible heat flux (Eq. (16)). This is used as an input file with surface temperature (Eq. (13)), soil heat flux (Eq. (15)) and surface net radiation (Eq. (2)) to

compute the instantaneous evapotranspiration (Eq. (19)) and the evaporative fraction (Eq. (18)). The evaporative fraction is then used with the surface albedo, 24 hour radiation and atmospheric transmissivity to compute the evapotranspiration (Eq. (21)).

Data analysis

The mean, standard error (SE) and coefficient of variation (CV) for each land use/cover type was computed for all the data using Microsoft office Excel. The variability of the data in the two catchments is assessed using the CV (equation 22).

$$CV = (\text{Standard Deviation}/\text{Mean}) 100 \tag{22}$$

Results and Discussion

Actual evapotranspiration distribution for Atankwidi catchment

Figure 2 illustrates the actual evapotranspiration distribution for the different images (November 11, 1989; November 7, 1999 and November 7, 2005) at Atankwidi catchment. Table 2 presents the mean and standard error of actual evapotranspiration by land use/cover types at Atankwidi catchment on November 11, 1989; November 7, 1999 and November 7, 2005.

Table 2: Mean actual evapotranspiration (ET_a), Standard Error (SE) and Coefficient of Variation (CV) by land use/cover types at Atankwidi catchment.

LULC Type	November 11, 1989			November 7, 1999			November 7, 2005		
	Mean (mm/ day)	SE	CV (%)	Mean (mm/ day)	SE	CV (%)	Mean (mm/ day)	SE	CV (%)
Closed woodlands	3.3	0.17	17	4.7	0.13	9	4.8	0.11	7
Open woodlands	2.8	0.29	33	3.9	0.21	20	4.4	0.13	12
Farmlands	2.8	0.23	31	4.9	0.17	14	4.7	0.09	8
Water bodies	6.3	0.22	13	6.8	0.13	7	6.9	0.11	6
Barelands	1.5	0.11	32	2.1	0.14	23	2.1	0.14	14
Rocky areas	2.0	0.13	25	3.7	0.14	10	4.3	0.06	6
Built-up areas	2.9	0.11	12	3.4	0.12	13	4.2	0.09	7

For the image acquired on November 11, 1989, high ET_a values were observed over water bodies and river beds while barelands, built-up and rocky areas had low values. Water bodies and barelands have the highest and lowest ET_a similar to the findings by [19], [Allen et al] and [Ahmad et al]. The mean ET_a across the different land use/cover types was 3.2 mm/day with a CV of 45%. The range of CV for ET_a across the different land use/cover types is 12–33%, falling within the ranges reported by [Ahmad et al] (5–47%), [Allen et al] (18–77%) and [19] (6–59%). Open

woodlands have the highest CV (33%) while built-up areas gave the lowest (12%). The CV of 32% for barelands is below the range (35–126%) reported by [19] but is similar to the 31% reported by [Allen et al]. The value of 13% for water bodies is higher than the 5% for water bodies in [Ahmad et al]. However, it falls within the range (6–30%) for water bodies reported by [19] and is similar to 18% for water bodies as reported by [Allen et al]. The value of 17% for closed woodlands is similar to the 15% obtained by [Ahmad et al] and also falls within the range (12–41%) as presented by [19]. Also the CV of 25% for rocky areas is within the range (19–40%) reported by [19].

For the November 7, 1999 image, high ET_a values were found in densely vegetated areas and low values in cultivated areas and barelands. Water bodies and barelands have the highest and lowest ET_a compared to the other land use/cover types as obtained by [19], [Allen et al] and [Ahmad et al]. The ET_a for built-up and rocky areas may be over estimated. According to [Compaore' et al], SEBAL overestimates the evaporation rate of bare lava flows in New Mexico and a similar observation has been made in Idaho [41]. On the other hand, this class also includes urban areas and settlements with trees, parks, vegetable gardens, and some lawns which contribute to evapotranspiration. The mean ET_a across these land use/cover types is 4.5 mm/day with a CV of 24%. The range of CV for the different land use/cover types is 7–23% and falls within similar ranges reported by [Ahmad et al] (5–47%), [Allen et al] (18–77%) and [19] (6–59%). Barelands have the highest CV (23%) while water bodies have the lowest CV (7%). The value of 7% for water bodies is less than the reported 18% by [Allen et al] but falls within the range (6–30%) reported by [19]. Also, the value of 9% for closed woodlands is similar to that of 12% by [19].

Based on the November 7, 2005 image, high ET_a values are also observed at water bodies, along rivers and dams and low values in cultivated areas and farmlands. The ET_a ranges from 4.2 mm/day for built-up areas to 6.9 mm/day for water bodies. Water bodies and barelands have the highest and lowest ET_a respectively compared to the other land use/cover similar to studies by [19], [Allen et al] and [Ahmad et al]. The mean ET_a across the different land use/cover types was 4.8 mm/day with a CV of 20%. The CVs range is 7–14% with barelands having the highest (14%) while water bodies and rocky areas have the lowest CV (7%). The value of 6% for water bodies is less than 18% reported by [Allen et al] but falls within the range (6–30%) reported by [19]. Also, the value of 8% for farmlands is similar to 10% reported by [Ahmad et al] for a similar land use/cover type.

In November (i.e. beginning of the dry season), the land is relatively moist, and most land use/cover types are found to evaporate water. Therefore the ET_a values were relatively high, and all land use/cover types were contributing to atmospheric humidity. The higher CV in the ET_a for the land use/cover types is due to the differences in transpiration and evaporation rates for the different land use/cover types. In the Atankwidi catchment, ET_a is observed to be higher on November 7, 2005 than in November 7, 1999 which was also higher than that of November 11, 1989 for each of the different land use/cover types. The only exception was that of farmlands on which November 7, 1999 was higher than November 7, 2005.

Actual Evapotranspiration (ET_a) distribution for Afram catchment

Illustrated on Figure 3 is the spatial distribution of surface albedo at the Afram catchment for the different images used. Also, presented on Table 3 are the mean surface albedo values for the different land use/cover types on January 11, 1986; March 20, 2002 and January 13, 2007.

Table 3: Mean actual evapotranspiration (ET_a), Standard Error (SE) and Coefficient of Variation (CV) by land use/cover types at Afram catchment.

LULC Type	January 11, 1986			March 20, 2002			January 13, 2007		
	Mean (mm/ day)	SE	CV (%)	Mean (mm/ day)	SE	CV (%)	Mean (mm/ day)	SE	CV (%)
Gallery Forests	5.6	0.14	11	3.1	0.28	35	6.1	0.20	13
Closed woodlands	5.4	0.14	12	2.7	0.08	13	6.2	0.02	12
Farmlands	5.9	0.03	9	2.5	0.07	13	6.1	0.06	14
Water bodies	7.3	0.10	5	1.4	0.31	72	6.8	0.02	6
Barelands	3.3	0.09	7	2.2	0.13	27	3.6	0.04	10
Built-up areas	5.2	0.08	7	2.2	0.20	43	5.7	0.05	11

For the January 11, 1986 image, high ET_a values were obtained in water bodies (7.3 mm/day) and low values in built up areas. As reported by [19], [Allen et al] and [Ahmad et al], water bodies and barelands have the highest and lowest ET_a respectively. The mean ET_a across the different land use/cover types was 5.8 mm/day with a CV of 13%. The range of CVs is 5–12% with closed woodlands having the highest CV (12%) while water bodies have the lowest CV (5%). The value of 5% for water bodies is lower than the range (6–30%) reported by [19] but the same as the 5% reported by [Ahmad et al]. Also, the value of 9% for farmlands is similar to 10% reported by [Ahmad et al] for a similar land use/cover type. The range of CV is within the range (5–47%) as presented by [Ahmad et al].

Based on the March 20, 2002 image, high ET_a values were obtained in gallery forest (3.1 mm/day) and low values in water bodies (1.4 mm/day). Contrarily to observations by [19], [Allen et al] and [Ahmad et al] water bodies have the lowest ET_a. This may however be due to the rainfall event on the day of image acquisition (March 20, 2002) since rainfall on or a few days before the day of image acquisition can significantly affect the ET_a estimated by the SEBAL model. The mean ET_a and CV across the different land use/cover types was 2.3 mm/day and 25%, respectively. The CVs range from 13–72% falls within range (6–59%) reported by [19] and is similar to the range (18–77%) by [Allen et al]. Water bodies have the highest CV of 72% while closed woodlands and farmlands have the same and lowest CV of 13%. The CV of 35% for gallery forest falls within the range reported by [19].

For the January 13, 2007 image, water bodies and bare lands had the highest and lowest ET_a values of 6.8 mm/day and 5.6 mm/day, respectively as reported by [19], [Allen et al] and [Ahmad et al]. The mean ET_a across the different land use/cover

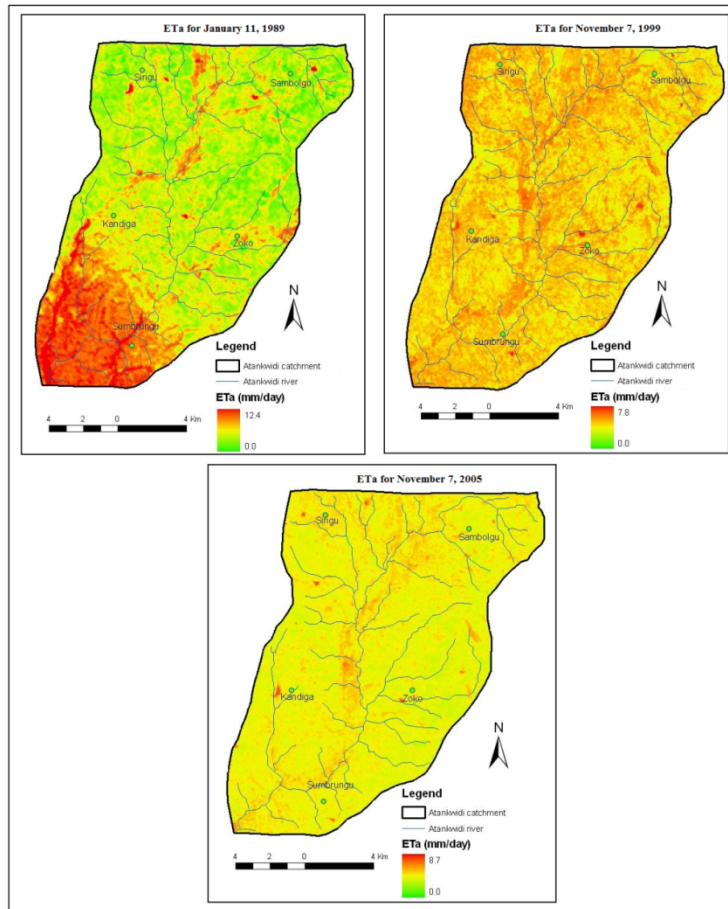


Figure 1: Actual Evapotranspiration maps of Atankwidi catchment.

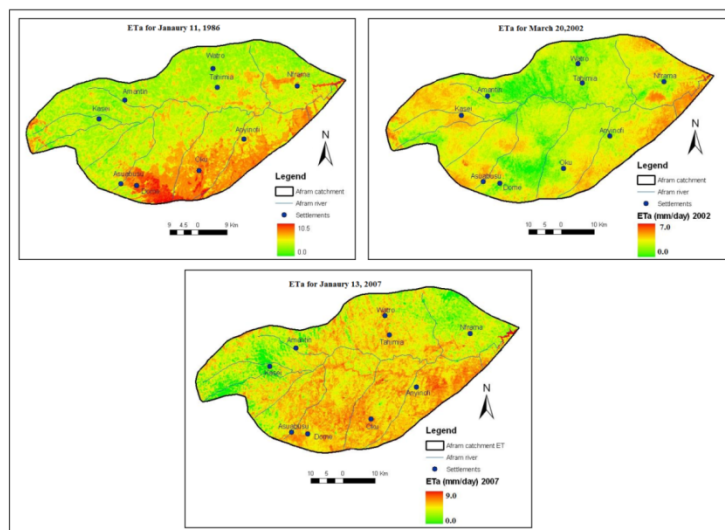


Figure 3: Actual Evapotranspiration maps of Afram catchment.

Conclusions

The study successfully estimated actual ET_a for different land use/cover types (closed woodlands, gallery forests, open woodlands, farmlands, water bodies, barelands, rocky areas and built-up areas) using 3 satellite images each for the Atankwidi and Afram catchments in the Volta Basin of Ghana. The study has shown that the SEBAL model can be conveniently used to estimate ET_a for different land use/cover in catchments similar to those of the study areas.

The ET_a values varied from 1.5 – 6.9 mm/day and 1.4 - 7.3 mm/day for the Atankwidi and Afram catchments respectively across the different land use/cover types. The range of CVs for ET_a was 5–75% across the different land use/cover types for the two catchments. In both catchments, it was observed that the mean CVs across the different land use/cover types were higher than the individual land use/cover (eg. open woodlands) CVs for ET_a . This means that the SEBAL model can be used to distinguish ET_a among the different land use/cover types in the two catchments. However, SEBAL estimates of ET_a are affected by rainfall as observed for the March 20, 2002 Afram catchment image resulting in higher CV for different land use/cover types.

The results shows that the SEBAL model gives reasonable estimates of ET_a and can also be used to distinguish different land use/cover types in the Volta Basin of Ghana.

References

- [1] Smith, M., 2000, "The application of climatic data for planning and management of Sustainable rain-fed and irrigated crop production," *Agric. For. Meteorol.*, 103, 99-108.
- [2] Oguntunde, P.G., 2004, "Evapotranspiration and complementarity relations in the water balance of the Volta Basin: Field measurements and GIS-based regional estimates," Centre for Development Research, University of Bonn, Bonn, Germany.
- [3] Mauser, W., and Schädlich, S., 1998, "Modelling the spatial distribution of evapotranspiration on different scales using remote sensing data," *Journal of Hydrology*, 212-213, 250-267.
- [4] Vörösmarty, C.J., Federer, C.A., and Schloss, A.L., 1998, "Potential evaporation functions compared on US watersheds: possible implications for global-scale water balance and terrestrial ecosystem modeling," *J. Hydrol.*, 207, 147-169.
- [5] Doorenbos, J., and Pruitt, W.O., 1977, *Crop water requirements*, FAO Irrigation and drainage paper n° 24, 2nd ed., Food and Agricultural Organization of UN, Rome, Italy.
- [6] Allen, R.G., Pereira, L.S., Raes, D., and Smith, M., 1998, "Crop Evapotranspiration. Guidelines for computing crop water requirements," FAO

- Irrigation and Drainage Paper 56, Food and Agricultural Organization of the United Nations, Rome, Italy.
- [7] Thomthwaite, C.W., and Mather, J.R., 1955, "The water balance Publications in climatology, " Centerton, NJ: Drexel Institute of Technology. Vol. VIII, No. 1.
- [8] Engman, E.T., and Gurney, R.J., 1992, Remote sensing in hydrology, Chapman and Hall, London.
- [9] Kustas, W.P., and Norman, J.M., 1996, "Use of remote sensing for evapotranspiration monitoring over land surfaces," *Hydrolog. Sci. J.*, 41 (4), 495-515.
- [10] Bastiaanssen, W.G.M., Menenti, M., Feddes, R.A., and Holtslag, A.A.M., 1998, "A remote sensing surface energy balance algorithm for land (SEBAL): 1. Formulation," *J. Hydrol.*, 212/213, 198-212.
- [11] Kustas, W.P., Diak, G.R., and Moran, M.S., 2003, *Evapotranspiration and Remote Sensing*, Encyclopedia of Water Science, Marcel Dekker, Inc., New York.
- [12] Pelgrum, H., and Bastiaanssen, W.G.M., 1996, "An intercomparison of techniques to determine the area-averaged latent heat flux from individual in situ observations: A remote sensing approach using the European Field Experiment in a desertification- threatened area data," *Water Resour. Bull.*, 32, 2775-2786.
- [13] Roerink, G.J., 1997, "Relating crop water consumption to irrigation water supply by remote sensing," *Water Resour. Manage.*, 11, 445-465.
- [14] Van de Hurk, B.J.J.M., Bastiaanssen, W.G.M., Pelgrum, H. and van Meijgaard, E. 1997, "A new methodology for assimilation of initial soil moisture fields in weather prediction models using Meteosat and NOAA data," *J. Appl. Meteor.*, 36: 1271-1283.
- [15] Allen, R.G., Morse A., Tasumi, M., Trezza, R., Bastiaanssen, W.G.M., Wright, J.L., and Kramber, W., 2002, "Evapotranspiration from a satellite-based surface energy balance for the Snake Plain Aquifer in Idaho," *Proceedings of the National USCID Conference*, San Luis Obispo, California, July 8-10, 2002.
- [16] Farah, H.O., 2001, "Estimation of regional evaporation under different weather conditions from satellite and meteorological data: A case study of the Navaisha Basin," PhD Thesis, ITC, Wageningen University.
- [17] Bastiaanssen, W. G. M., and Chandrapala, L., 2003, "Water balance variability across Sri Lanka for assessing agricultural and environmental water use," *Agric. Water Manage.*, 58 (2), 171-192.
- [18] Bastiaanssen, W.G.M., Ahmad, M.D., and Chemin, Y., 2002, "Satellite surveillance of evaporative depletion across the Indus Basin," *Water Resour. Res.*, 38 (12), 1273-1282.
- [19] Compaore', H., 2006, "The impact of savannah vegetation on the spatial and temporal variation of the actual evapotranspiration in the Volta Basin, Navrongo, Upper East Ghana," *Centre for Development Research*, University of Bonn, Bonn, Germany.

- [20] Compaore', H., Hendrickx, J.M.H., Hong, S., Friesen, J., van de Giesen, N.C., Rodgers, C., Szarzynski, J., and Vlek, P.L.G., 2007, "Evaporation mapping at two scales using optical imagery in the White Volta Basin, Upper East Ghana," *Physics and Chemistry of the Earth*, doi: 10.1016/j.pce.2007.04.021.
- [21] Tucker, C.J., 1979, "Red and photographic infrared linear combination for monitoring vegetation," *Remote Sens. Environ.*, 8: 127-150.
- [22] Bastiaanssen, W.G.M., 1995, "Regionalisation of surface flux densities and moisture indicators in composite terrain," PhD thesis, Wageningen Agricultural University, Wageningen, The Netherlands.
- [23] Campbell, G.S., and Norman, J.M., 1998, *An introduction to environmental biophysics*. Second Edition, Springer, New York, NY.
- [24] Bastiaanssen, W.G.M., 2000, "SEBAL-based sensible and latent heat fluxes in the irrigated Gediz Basin, Turkey," *J. Hydrol.*, 229(1-2), 87-100.
- [25] NASA., 2002, *The Landsat-7 Science Data User's Handbook*.
- [26] Wukelic, G.E., Gibbons, D.E., et al., 1989, "Radiometric calibration of Landsat thematic mapper thermal band," *Remote Sensing of Environment*, 28: 339-347.
- [27] Brutsaert, W., Hsu, A.Y. and Schmugge, T.J., 1993, "Parametrization of surface heat fluxes above forest with satellite thermal and boundary layer soundings," *J. Appl. Meteorol.*, 32: 909-917.
- [28] Hong, S., 2008, "Mapping regional distributions of energy balance parameters using optical remotely sensed imagery," PhD Thesis, New Mexico Tech, Socorro NM.
- [29] Brutsaert, W., 1982, *Evaporation into the atmosphere: theory, history and applications*, Reidel, Dordrecht.
- [30] Brutsaert, W., and Sugita, M., 1992, "Application of self-preservation in the diurnal evolution of the surface energy budget to determine daily evaporation," *Journal of Geophysical Research*, 97 (17), 18,322-18,377.
- [31] Crago, R.D., 1996, "Conservation and variability of the evaporative fraction during the daytime" *Journal of Hydrology*, 180, 173-194.
- [32] Farah, H.O., Bastiaanssen, W.G.M., and Feddes, R.A., 2004, "Evaluation of the temporal variability of the evaporative fraction in a tropical watershed," *International Journal of Applied Earth Observation and Geoinformation*, 5, 129-140.
- [33] Shuttleworth, W.J., Gurney, R.J., Hsu, A.Y., and Ormsby, J.P., 1989, "FIFE: the variation in energy partitioning at surface flux sites," *IAHS Red Book Series no.*, 186, 67-74.
- [34] Martin, N., 2006, "Development of a water balance for the Atankwidi catchment, West Africa—A case study of groundwater recharge in a semi-arid climate," Centre for Development Research, University of Bonn, Bonn, Germany.
- [35] Agyare, W.A., 2004, *Soil characterization and modeling of spatial distribution of saturated hydraulic conductivity at two sites in the Volta basin of Ghana*, Centre for Development Research, University of Bonn, Bonn, Germany.

- [36] Adu, S.V., and Mensah-Ansah, J.A., 1995, "Soils of the Afram basin: Ashanti and Eastern regions, Ghana," CSIR - Soil Research Institute Memoir no., 12, 17-53.
- [37] Codjoe, S. N.A., 2004, "Population and Land Use/Cover dynamics in the Volta River Basin of Ghana, 1960-2010," Centre for Development Research, University of Bonn, Bonn, Germany.
- [38] Adu, S.V., 1969, "Soils of the Navrongo-Bawku Regions," Memoire no. 5, CSIR-soil Research Institute.
- [39] Allen, R., Tasumi, M., and Trezza, R., 2007, METRICT: Mapping Evapotranspiration at High Resolution. Applications Manual for Landsat Satellite Imagery, Version 2.0.3, University of Idaho, Kimberly, Idaho.
- [40] Ahmad, M.D., Biggs, T., Turrall, H., and Scott, C.A., 2006, "Application of SEBAL approach and MODIS time-series to map vegetation water use patterns in the data scarce Krishman river basin in India," *Water Science and Technology*, 53(10), 83-90.
- [41] Tasumi, M., 2003, "Progress in operational estimation of regional evapotranspiration using satellite imagery," PhD Thesis, University of Idaho, Moscow, Idaho.